



Surface feature and material removal in ultrasonic vibration-assisted slot-milling of Ti–6Al–4 V titanium alloy

Baoqi Chang^{1,2} · Zhaoxi Yi^{1,2} · Xiaobing Cao^{1,2} · Ji-an Duan^{1,2}

Received: 10 March 2022 / Accepted: 30 May 2022 / Published online: 30 August 2022
© The Author(s), under exclusive licence to Springer-Verlag London Ltd., part of Springer Nature 2022

Abstract

The continuous optimization of processing technology and evaluation methods is an important way to achieve high processing quality and processing efficiency for difficult-to-process materials. To solve the problem of frequent defects in the slot, the ultrasonic vibration-assisted slot-milling (UVASM) technology was developed for processing titanium alloy. Simultaneously, comparative experiments were carried out between UVASM and conventional slot milling (CSM), in terms of surface features of slot bottom and slot sidewall, cutting force, tool trajectory, chip morphology, and micro-hardness. The results show that uniform vibration micro-texture could significantly improve surface topography of slot bottom in UVASM, while numerous tool feed trajectories and observable machining defects detract from the surface quality in CSM. The UVASM can greatly reduce material spalling and edge breakage, thereby maintaining a smooth and regular edge profile of the slot sidewall. The tool tip trajectories of the two machining methods are highly corresponding to the machining textures of the slot sidewall surface. There is a high-frequency and small-amplitude force fluctuation signal on the axial force waveform in UVASM, which can reduce the instantaneous maximum milling force and milling force in the stable stage by 8.7 and 12.2%, respectively. The UVASM has a better chip breaking effect and surface anti-scratch effect, and the UVASM can obtain higher surface micro-hardness and deeper plastic deformation layer than those CSM. In summary, the multi-dimensional evaluation of slot processing status has been completed, and the processing quality of the slot has been improved.

Keywords Ultrasonic vibration-assisted slot milling · Slot sidewall · Chip morphological · Micro-texture · Subsurface micro-hardness

1 Introduction

Structural parts that are manufactured from titanium alloys have low density, high specific stiffness, high strength, high fatigue resistance, and high corrosion resistance, which makes them valuable in the aerospace industry [1–3]. Titanium alloys are reportedly commonly used as structural materials and aircraft fuselage skins in the aerospace industry, with approximately 14% of the Boeing 787's

fuselage being made of titanium alloys [4, 5]. In medical technology, biocompatible and highly wear-resistant materials are required for the manufacture of implants and endoprotheses (e.g., teeth, hip, or knee joints) [6]. For structural components of Ti–6Al–4 V, the material removal by machining can be up to 95% of the total workpiece mass [7]. The machining of workpieces made of titanium alloys inevitably involves corner machining and slot machining, which requires the uniform removal of material in the slot bottom while at the same time requiring the quality of the machining in the slot sidewalls [8]. However, it is difficult to guarantee the quality of both the slot bottom and the slot sidewall with conventional machining methods [7, 9]. Moreover, machining defects are often found on the slot sidewalls, which can lead to the overall failure of the workpiece. Titanium alloy forming and processing is extremely difficult because of its high strength and high specific stiffness, leading to tool wear and irregular material removal phenomenon. Irregular material removal will lead

✉ Zhaoxi Yi
yizhaoxi_academy@163.com

✉ Ji-an Duan
duanjian@csu.edu.cn

¹ State Key Laboratory of High Performance and Complex Manufacturing, Central South University, Changsha 410083, China

² College of Mechanical and Electrical Engineering, Central South University, Changsha 410083, China

to increased surface roughness and processing defects, which will eventually lead to surface cracks and workpiece failure [10–12]. Therefore, reducing the processing defects and improving the uniformity of material removal is vital to improve machining performance and extend the service life of the workpiece for difficult-to-process materials. Meanwhile, it would be of great research and practical value to investigate a processing technology and its processing mechanism that can guarantee the quality of both the slot bottom and the slot sidewall.

Generally, evaluation criteria for the surface feature include micro-hardness, surface topography, surface roughness, and residual stress [13]. At the same time, the material removal characteristics directly affect the evaluation parameters of surface features. Therefore, it is necessary to investigate the performance characteristics of material removal and surface features as well as the correlation between them. The excellence of ultrasonic-assisted machining technology in machining difficult-to-process materials has been reported and recognized in literature [14–17]. Therefore, this paper presents an exploratory study on UVASM of Ti–6Al–4 V to better improve machining performance and meet the increasing functional requirements of aerospace components.

Literature [18–20] has proven that the uniform micro-textures obtained by the coupling effect of various vibration parameters and machining parameters were beneficial to improving surface properties. Ni and Zhu [21] studied the machining results of conventional milling (CM) and UVAM in terms of milling force, surface topography, and surface profile. The results showed that the cutting force features are richer and the cutting force is smaller in UVAM conditions than that in CM due to the intermittent cutting mechanism. Chen et al. [22] investigated the textured surface generation mechanism in vibration-assisted milling through modeling and experimental approaches. It is found that vibration-assisted milling is an effective method to generate certain surface textures (fish-scale textures) with controllable wettability. Liu et al. [23] investigated the effects of rotary ultrasonic elliptical machining for side milling (UEMSM). The results showed that UEMS significantly improved plastic deformation and work hardening. But at the same time, the ultrasonic vibration perpendicular to the machined surface would lead to the deterioration of surface roughness to a certain extent. Chen et al. [24] researched the material removal mechanism of ultrasonic vibration helical milling by modeling the cutting trajectories and peripheral cutting edges. The results showed that the cutting trajectories of bottom and peripheral cutting edges were consistent with the machined surface texture.

Chip formation and its morphology are important features of processing and generate important information about the cutting process itself [25–27]. Jung et al. [28] found the

phenomenon of chip segmentation in ultrasonic elliptical vibration cutting of Ti–6Al–4 V titanium alloy, which led to the forced vibration of the workpiece. Meanwhile, it is also found that the average uncut chip thickness and cutting width had a relation to the frequency and magnitude of the forced vibration. Ren et al. [29] studied the chips morphological in ultrasonic UVAM and CM of Ti–6Al–4 V alloy. Research indicated that the chips fragment of CM was severely deformed and the fragment edge was staggered, while the chips surface texture of UVAM was more uniform and the edge of the chip was smoother. The literature showed that the fatigue life of components was mainly determined by work hardening and grain refinement [30, 31]. Chen et al. [32] compared the subsurface hardness between ultrasonic vibration helical milling (UVHM) and helical milling (HM) of Ti–6Al–4 V alloy. Results indicated that UVHM generates higher surface hardness at the subsurface of machined holes (20–200 μm) than that of HM. Additional research has proved that ultrasonic vibration machining can generate a greater work hardening effect at the subsurface and surface, thereby increasing the surface hardness and extending the fatigue life of the workpiece (e.g., titanium alloy, carbon steel) [33–35]. Abdo et al. [9] analyzed the surface topography and edge chipping on the channel bed and channel sidewall of microchannels in rotary ultrasonic milling of biolox forte ceramic. The results indicate the presence of more brittle fractures and deep pits in the channel bed compared to the channel sidewalls. Similarly, researchers will simultaneously evaluate the processing state of the bottom and the inner wall of the hole to ensure the overall processing quality in hole processing [36, 37]. Results show that slot sidewall is the location where machining defects are prone to occur in slot milling and the investigation of its machining quality is extremely essential.

Literature review shows that there is a paucity of literature focusing on the machining quality of slot bottom and slot sidewall simultaneously in the milling of Ti–6Al–4 V alloy. In addition, the problem of machining defects in slot milling of titanium alloys remains to be studied and solved. In this study, a theoretical analysis of the fundamental mechanism of separate-type machining and material removal is implemented first. Subsequently, the UVASM and CSM experiments were implemented to characterize various aspects of the slot milling surface and sub-surface machining state in terms of surface features and material removal direction.

2 Kinematics analysis of UVASM

Ultrasonic machining is usually regarded as a separate-type cutting method, where a large number of periodic separations and contacts between tool tips and workpiece

occur during the machining process [38]. The direction in which the ultrasonic vibration is applied determines the trajectory of the tool and the way of material removal. Different vibration forms will produce different processing textures and chip shapes.

As shown in Fig. 1a, this article applies ultrasonic longitudinal vibration to the axial direction of the milling cutter. The cutting process will not be limited by the critical cutting speed due to the application direction of ultrasonic vibration. It can achieve complete tool-workpiece high-frequency separation cutting during the processing. The ultrasonic milling of the rectangular slot is completed by the four-flute milling cutter along the path shown by the dashed line in Fig. 1a, b shows the process of microscopic material removal in ultrasonic milling. The tip of the milling cutter cuts on the material matrix in a sinusoidal curve, and the overlapping of the cutting paths at different times forms different chip shapes. The formations of thinner and shorter chips in different conditions are due to separate-type cutting in the UVASM process.

Generally, the displacement and velocity functions of the ultrasonic vibration signal can be expressed as Eq. (1).

$$\begin{cases} X = A \sin \omega t \\ v = A\omega \cos \omega t \end{cases} \quad (1)$$

where A denotes the ultrasonic vibration amplitude, $\omega = 2\pi f$ denotes the angular frequency, and f denotes the vibration frequency of the ultrasonic vibration signal, respectively.

According to Eq. (1), the displacement curve of ultrasonic vibration is illustrated in Fig. 2. It can be observed from Fig. 2 that the ultrasonic milling process can be divided into the cutting stage and separation stage in a vibration cycle. Figure 3 shows the illustration of the tool-workpiece separation-contact cutting process during an ultrasonic vibration cycle. Assume that t_0 is the critical moment when the cutting edge of the milling cutter contacts the workpiece,

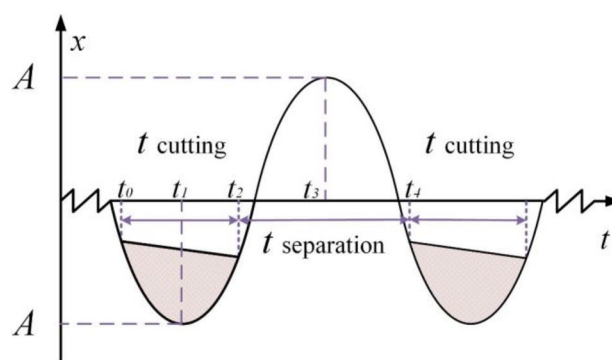


Fig. 2 Displacement curve of ultrasonic vibration

and that the vibration direction of the cutting edge is toward the workpiece. At t_1 , the cutting edge cuts into the workpiece with the action of ultrasonic vibration and reaches the maximum cutting depth D_{max} . At this time, the vibration direction of the cutting edge changes from toward the workpiece to away from the workpiece, and subsequently, the cutting edge gradually separates from the workpiece. At t_2 , the cutting edge moves to the original cutting depth position and continues to move away from the workpiece. At t_3 , the cutting edge moves to the farthest position d_{max} from the workpiece. From t_3 to t_4 , the cutting edge moves toward the workpiece and finally reaches the critical state of contact with the workpiece. Therefore, it can be concluded that a complete cutting cycle in UVASM is from time t_0 to t_4 .

In addition, this paper finds that the tool-workpiece separation-contact behavior contributes to the chip breaking effect. In the last picture of Fig. 3, the cutting edge is in a critical state just contacting the workpiece, and the direction of ultrasonic vibration is away from the workpiece. During the cutting process, the removed chips are mainly formed by the extrusion of cutting force F_C , which is the same as the CSM. In addition, the chips are

Fig. 1 a UVASM process with a four-flute end mill; b schematic of material removal.

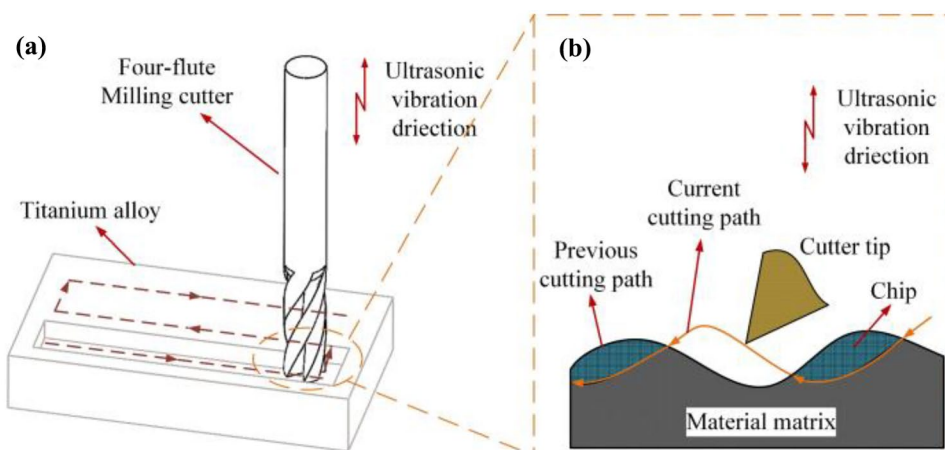
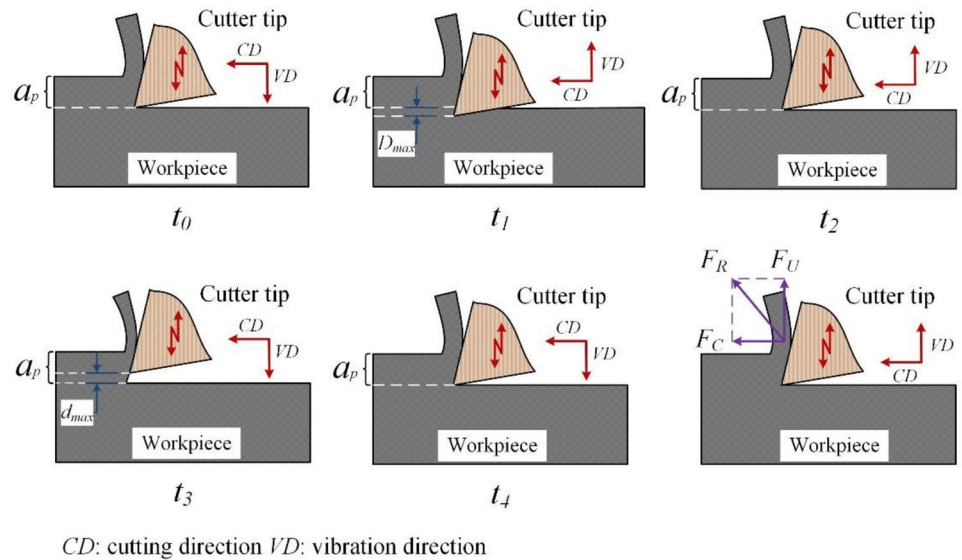


Fig. 3 Visualization of tool-workpiece separation-contact in UVASM



also subjected to the additional cutting force generated by the resonance cutter tip in the UVASM process. Obviously, the additional cutting force F_U generated by ultrasonic vibration significantly promotes the chip breaking effect compared with CSM processing. The chip breaking effect helps to produce relatively short chips with uniform texture topography, which will be analyzed and discussed in the next section.

3 Experimental setup and procedures

The UVASM and CSM experiment for Ti-6Al-4 V titanium alloy were carried out on a machining center JDGR200T with the maximum spindle speed 20,000 rpm. The experimental system of UVASM and CSM is shown in Fig. 4. As shown in Fig. 4, the titanium alloy workpiece and the dynamometer were fixed on the platform of the

machining center, and the ultrasonic vibration system was clamped on the spindle to provide a certain frequency of ultrasonic excitation for the tool. The ultrasonic vibration system was composed of an ultrasonic generator, a wireless transmission ring, and an ultrasonic cutter shank, which applied axial ultrasonic vibration to the milling cutter. Dynamometer (Kistler-9257B), charge amplifier (Kistler-5070A), and DAQ system were used to measure cutting force during machining.

The experimental conditions are summarized in Table 1. The laser displacement sensor (LK-H020) was used for measuring the amplitude of the front end of the milling cutter. And different amplitudes can be obtained by adjusting the power of the ultrasonic generator. The resonant frequency of the system after clamping the milling cutter was approximately 28 kHz. The corresponding relationship between the tool amplitude and the power of the ultrasonic generator is shown in Table 2.

Fig. 4 Experiment system

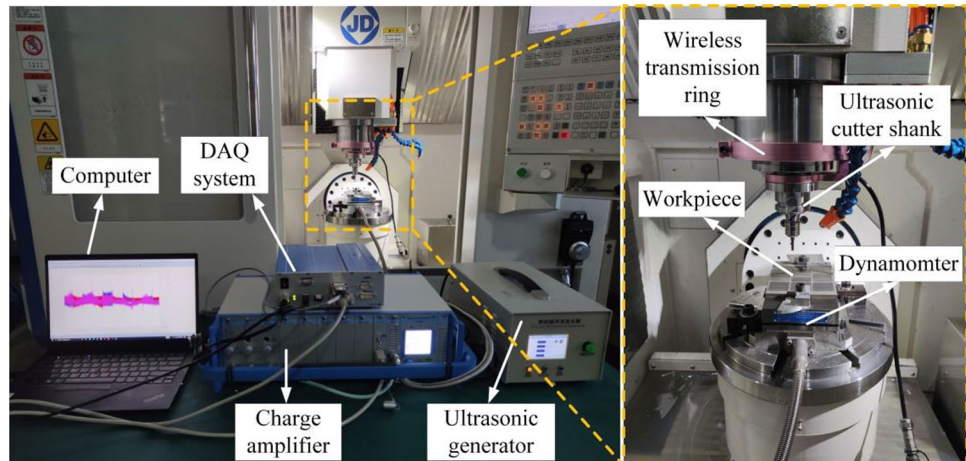


Table 1 Experimental conditions

Tool		Workpiece	
Tool type	Four-flute end mill	Workpiece material	Ti-6Al-4 V
Tool material	TiAlN carbide	Workpiece dimension	110 mm × 100 mm × 5 mm
Tool diameter	4 mm	Milling area	30 mm × 15 mm
Helix angle	38 and 41°	Milling area depth	Table 3

The UVASM and CSM experiments were established in wet conditions with cutting fluid. The switching between the UVASM and CSM experiments can be realized by switching the ultrasonic generator on and off. The UVASM and CSM experiments’ processing parameters are listed in Table 3. The spindle rotation speed is 4000 rpm.

After the milling experiment, the surface topography and chip morphology were detected using an ultra-depth microscope (VHX-5000). A white-light interferometer (WYKO NT9100) was used to measure the three-dimensional profile and roughness of the milled surface. Hardness values at different depths from the machined surface were tested by a MHV digital micro-hardness tester (type: 2000) using a load of 5 N for 10 s duration.

4 Results, analysis, and discussion

4.1 Machined surface profile and geometrical texture of slot bottom

The overall processing quality evaluation of slot-milling includes the evaluation of the slot bottom and the slot side wall. To evaluate the machined surface quality of slot bottom, surface profile, surface roughness, and geometrical texture in UVASM and CSM were tested for different machining conditions.

The movement of the cutting tool directly determines the material removal mode and the geometric micro-texture of the machined surface. The surface topography detected by the ultra-depth microscope is presented in Fig. 5.

Figure 5 shows the surface topographies characteristics of UVASM and CSM with different cutting depths. As shown in Fig. 5a, b, c, and d, a multitude of scratches appear on the surface of CSM and the depth and width of scratches increase to varying degrees with the increase of cutting

depth. When $a_p = 0.08$ mm, the machining defects on the CM surface begin to appear, which manifest as irregular material removal. When the cutting depth increases to $a_p = 0.10$ mm, the irregular material removal is intensified, which causes the local processing defects to evolve into multi-position pit-shaped surfaces. Moreover, the tool trajectory and cutting width trace almost completely disappear. The cause of local processing defects and the pit-shaped surface is that the material is not removed evenly and completely following the motion trajectory of the cutting edge but falls off or peels off in pieces.

As shown in Fig. 5e, f, g, and h, the UVASM surface exhibits regular ultrasonic vibration texture, clear tool trajectory, and obvious cutting width. When the cutting depth increases, the integrity and uniformity of ultrasonic vibration texture can be maintained. However, when $a_p = 0.08$ mm, slight machining defects also appear on the machined surface. Observation and analysis found that the ultrasonic vibration in the axial direction does not change the motion trajectory of the tool in the feed direction but increases the high-frequency intermittent contact and separation of the tool-workpiece in the axial direction of the tool, which is manifested as dense ultrasonic action points on the machined surface. As a result, the dynamic change of the

Table 2 Correspondence between ultrasonic generator power factor and tool amplitude

Power factor/%	Amplitude/ μm
60	1.6
70	2.6
80	2.8
90	3.1

Table 3 Experimental conditions of UVASM and CSM

Exp. no	Feed speed v_f /mm/min	Cutting depth a_p / μm	Cutting width a_d / μm	Power factor p /%
1	100	0.06	0.2	80, 0
2	200			
3	300			
4	400			
5	200	0.04	0.2	80, 0
6		0.08		
7		0.1		
8	200	0.06	0.5	80, 0
9			0.8	
10			1.1	
11	200	0.06	0.2	60
12				70
13				90

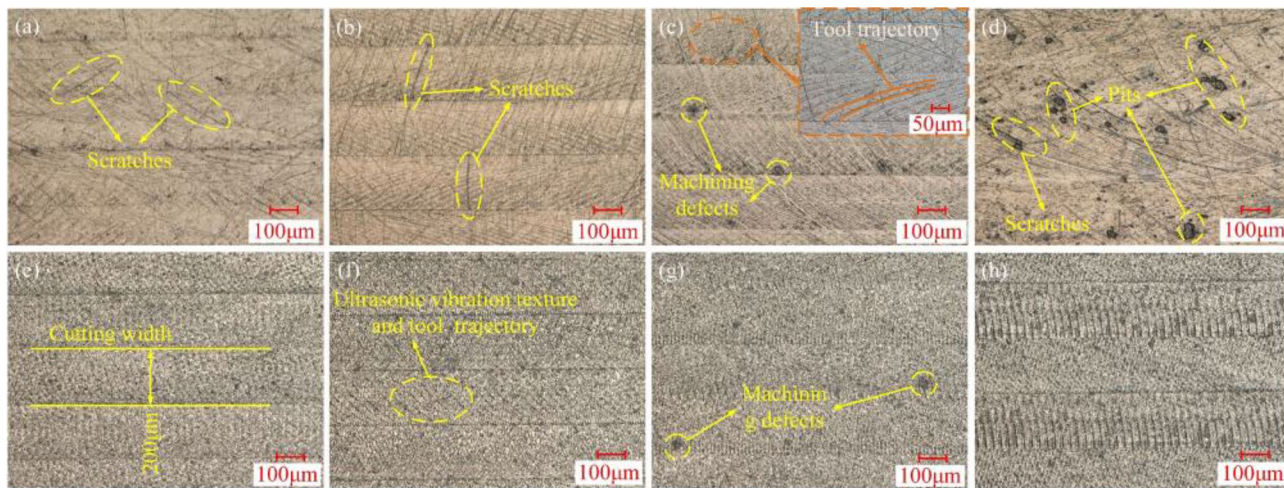


Fig. 5 Surface topography under different machining conditions: **a** $a_p=0.04$ mm, CSM, **b** $a_p=0.06$ mm, CSM, **c** $a_p=0.08$ mm, CSM, **d** $a_p=0.10$ mm, CSM, **e** $a_p=0.04$ mm, UVASM, **f** $a_p=0.06$ mm,

UVASM, **g** $a_p=0.08$ mm, UVASM, and **h** $a_p=0.10$ mm, UVASM (exp. no. 5, no. 2, no. 6, and no. 7)

cutting thickness in UVASM is achieved, so that the material can be removed with a smaller cutting amount during the machining process. In addition, the high-frequency intermittent of the tool-workpiece processing method can promote the penetration of cutting fluid into the cutting area, taking away the chips to prevent scratching the machined surface. Therefore, UVASM can make the material removal process more refined and uniform, thereby forming a clean and uniform processing surface.

The microscopic removal mechanism of materials is an important factor affecting the surface quality. Statistics show that the adjacent area of the cutting width is the high-frequency zone where processing defects occur,

especially in CSM, and the material is more likely to peel off and form a pit-shaped surface. It shows that the material can be removed evenly and completely following the motion trajectory of the cutting edge and the ultrasonic vibration trajectory in UVASM. Comparing the surface topographies in UVASM and CSM, the UVASM method can greatly avoid the scratches of the machined surface and reduce the formation of processing defects. Therefore, uniform micro-textures in the UVASM method significantly improve the topography of the machined surface, where a multitude of uniform micro-textures replace disordered tool marks and machining defects that occur on CSM surfaces.

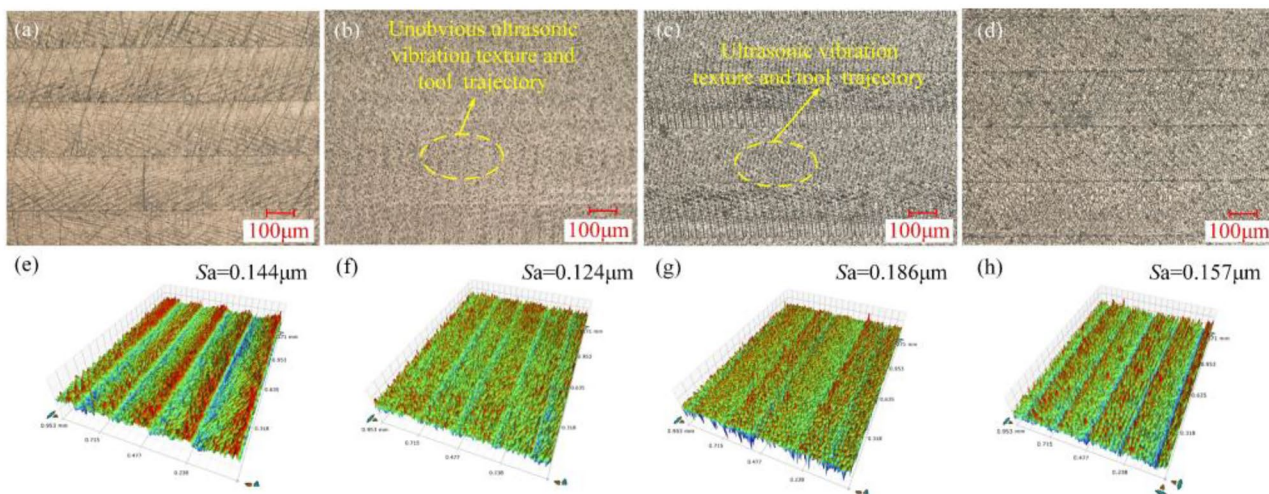


Fig. 6 Surface topography of 2D and 3D under different ultrasonic power: **a** $p=0$, 2D, **b** $p=60\%$, 2D, **c** $p=70\%$, 2D, **d** $p=80\%$, 2D, **e** $p=0$, 3D, **f** $p=60\%$, 3D, **g** $p=70\%$, 3D, and **h** $p=80\%$, 3D (exp. no. 2, no. 11, and no. 12)

Figure 6 shows the two-dimensional (2D) and three-dimensional (3D) topographies characteristics of the machined surface under the same milling parameters and different ultrasonic power. The zero of ultrasonic power represents the CSM. As shown in Fig. 6e, the CSM surface shows obvious tool trajectory and cutting width, and the surface roughness is 0.144 μm. As shown in Fig. 6b, unobvious ultrasonic vibration texture and tool trajectory appear on the machined surface when the ultrasonic power is 60%. Accordingly, the tool axial vibration forms an undulating profile with a small height on the surface in Fig. 6f. A profile with a small undulation degree represents a low surface roughness value ($S_a=0.124 \mu\text{m}$). With the increase of ultrasonic power, the axial amplitude of the tool increases, and the ultrasonic vibration texture and tool trajectory become clear and complete. At the same time, the tool with ultrasonic vibration creates many machining marks on the surface, such as “peak” and “trough,” which aggravates the surface undulation. When the ultrasonic power is 70 and 80%, the surface roughness is 0.186 and 0.157 μm, respectively.

As shown in Fig. 7, there is a more undulating profile in the direction perpendicular to the machined surface in UVASM than that of CSM. A profile curve with a smaller peak value caused by small ultrasonic amplitude represents a lower roughness value. When the ultrasonic amplitude increase, the peak value of the surface profile curve becomes larger, leading to an increase in the roughness value. When

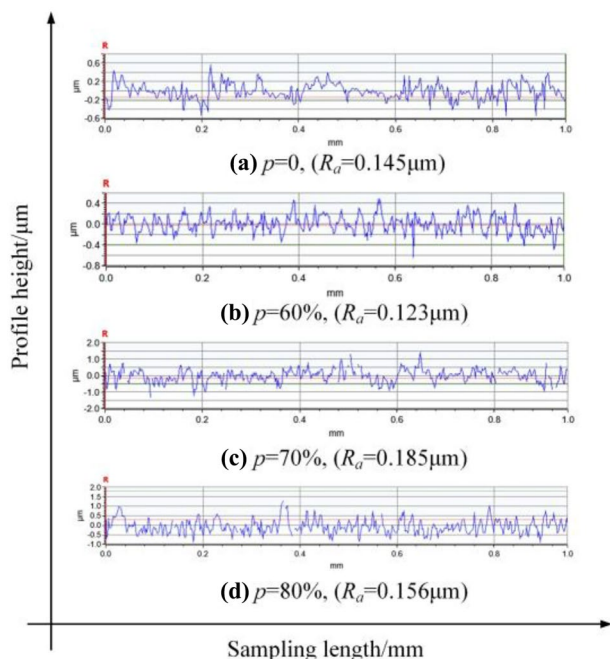


Fig. 7 Profile curve in vertical feed direction under different ultrasonic power (exp. no. 2, no. 11, and no. 12)

ultrasonic vibration is applied in the direction perpendicular to the machining surface, the magnitude of the ultrasonic amplitude will directly affect the profile curve and roughness of the machined surface. The larger the ultrasonic amplitude does not mean the smaller the surface roughness. Therefore, it is necessary to select the appropriate ultrasonic amplitude and processing parameters to match the relationship between them, thereby obtaining a lower surface roughness.

4.2 Topography and profile of slot sidewall

In slot milling, machining defects usually occur at the slot sidewalls that affect the overall machining quality, such as edge chipping and material spalling. Therefore, it is essential to carry out a comprehensive evaluation of the machining quality of slot sidewalls.

4.2.1 Analysis of tool trajectory

Because the position of the tool relative to the slot bottom and sidewall is different, the tool trajectories formed by the tool tips on the slot bottom and the slot sidewall are different. The motion trajectories of tool tips on the slot sidewall during the CSM and UVASM process can be expressed as Eqs. (2) and (3) [21], respectively.

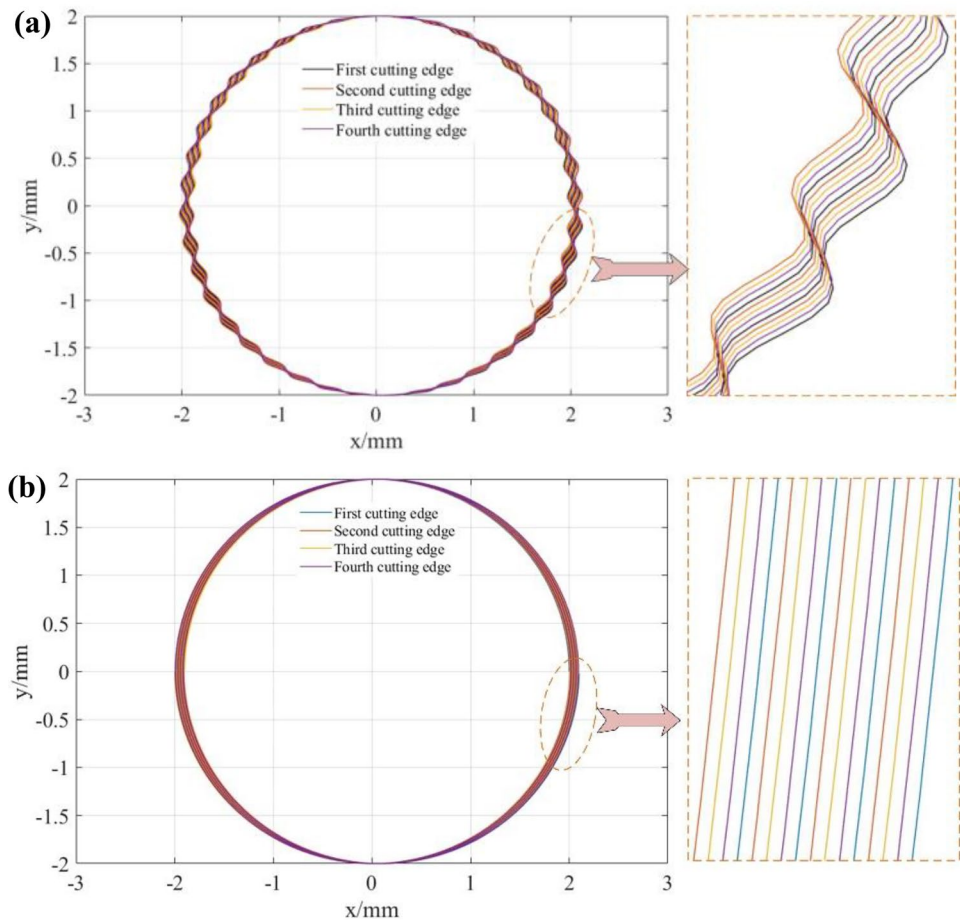
$$\begin{cases} x = R \cos(\omega t - \frac{2\pi(Z_i - 1)}{N}) + v_f t \\ y = R \sin(\omega t - \frac{2\pi(Z_i - 1)}{N}) \end{cases} \quad (2)$$

$$\begin{cases} x = R \cos(\omega t - \frac{2\pi(Z_i - 1)}{N}) + v_f t + A \sin(2\pi f + \theta) \\ y = R \sin(\omega t - \frac{2\pi(Z_i - 1)}{N}) \end{cases} \quad (3)$$

where R denotes the milling cutter radius, ω denotes the spindle angular velocity, v_f denotes the feed rate, f denotes the resonant frequency of the ultrasonic system, N is the number of flutes, Z_i ($i = 1, 2, 3, 4$) is the sequence number of cutting edges, and θ is the phase difference between adjacent waveforms.

The motion trajectories of tool tips in CSM and UVASM described by the above formulas are shown in Fig. 8. As shown in Fig. 8, the local magnified motion trajectories of the cutting edge in UVASM are similar to sine curves, while that of CSM are adjacent straight lines. In UVASM, the cutting edge performs high-frequency intermittent milling with a sinusoidal trajectory, forming the constantly changing dynamic cutting thickness. Compared with CSM, the approximately straight cutting trajectory represents the constant cutting thickness. Therefore, the introduction of ultrasonic vibration can refine the material removal process and reduce the cutting force to a certain extent.

Fig. 8 Motion trajectories of tool tips in CSM and UVASM: **a** trajectory in UVASM and **b** trajectory in CSM



As shown in Fig. 9, the milling force signal along the tool axial direction is mainly divided into the initial cutting stage and the stable cutting stage. In the initial cutting stage, the tool continuously cuts into the workpiece material until it reaches the

predetermined cutting depth and then enters the stable cutting stage. In the initial cutting stage of CSM, the instantaneous maximum milling force is $F_{z\max} = 141.6$ N, and the duration of the initial cutting stage is $t = 2.1$ s. Correspondingly, in the

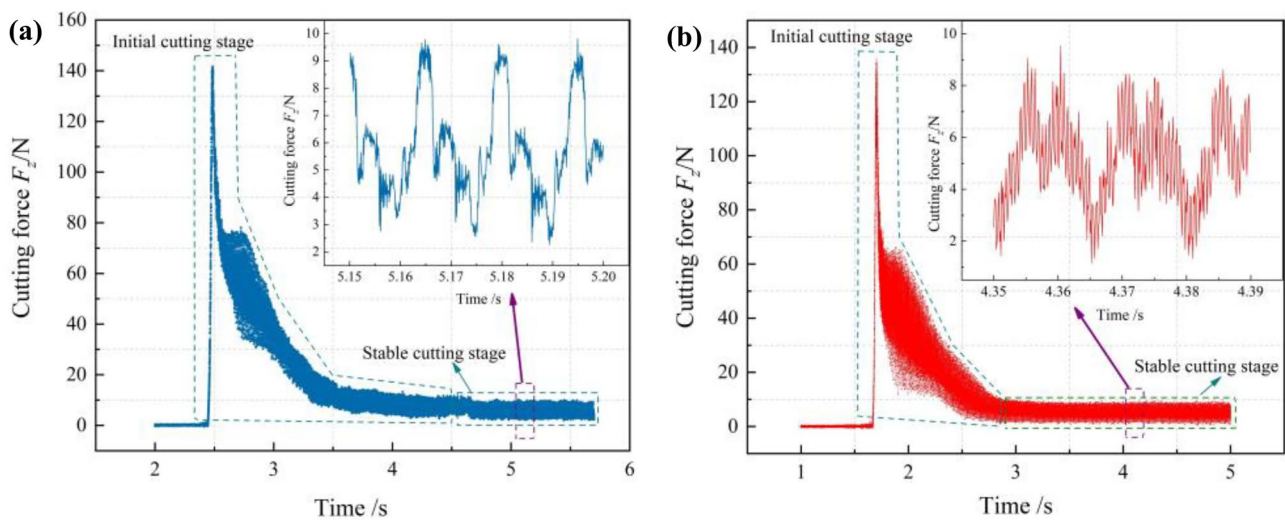


Fig. 9 Comparison of milling force F_z between **a** F_z in CSM and **b** F_z in UVASM (exp. no. 9)

initial cutting stage of UVASM, the instantaneous maximum milling force is $F_{zmax} = 129.3$ N, and the duration of the initial cutting stage is $t = 1.2$ s. Compared with CSM, the instantaneous maximum milling force and duration of the initial cutting stage in UVASM are reduced by 8.7 and 42.9%, respectively. By enlarging the milling force in the stable cutting stage, it can be found that the milling force waveform in UVASM has a high-frequency and small-amplitude force fluctuation signal on the original periodic vibration waveform. In CSM, the milling force waveform is composed of a similar sine wave and clutter waveform caused by the rotating cutting edge. This shows that there are high-frequency contact and separation between the tool-workpiece during the entire milling process in UVASM, forming a unique combination of high-frequency intermittent cutting force and sinusoidally changing milling force. Analyzing the milling force in the stable stage, it is found that the milling force ($F_z = 8.6$ N) in UVASM is reduced by 12.2% compared to the CSM force ($F_z = 9.8$ N).

4.2.2 Analysis of the processing quality of the slot sidewall

As shown in Fig. 10, Fig. 10c illustrates a schematic view of a single slot divided by WEDM in Fig. 10b. Figure 10d is a topography of the slot sidewall edge taken with an ultra-depth microscope in the direction perpendicular to the slot sidewall, corresponding to Figs. 11 and 12. Correspondingly, Fig. 10a presents a profile curve of the slot sidewall edge taken in cross-section in the top view direction of the slot sidewall by the ultra-depth microscope, corresponding to Fig. 13.

It can be observed that the surface textures in Fig. 11 are highly consistent with the simulated tool trajectories in Fig. 8. In CSM, the adjacent cutting lines at different times generate the machined surface with obvious tool feed trajectories. In contrast, relative uniform vibration micro-texture appears on the machined surfaces due to the application of ultrasonic vibration in UVASM. Therefore, it could be concluded that the machined surface topographies are mainly governed by tool trajectories in both CSM and UVASM methods, depending on the tool tips trajectories in Fig. 8 and surface topographies in Fig. 11.

Figure 12 shows the topographies of the slot sidewall edge in UVASM and CSM under different cutting depths, and Fig. 13 shows the profile curve of the slot sidewall edge with corresponding parameters obtained in cross-section in the top view direction of the sidewall. As shown in Fig. 12, the sidewall surface shows obvious tool feed trajectories in CSM, while that of UVASM is uniform ultrasonic vibration trajectories. In Fig. 12a, c, e, and g, edge breakage and edge crack occur on the edge of the sidewall in CSM. When $a_p = 0.10$ mm, a lot of material spalling and edge breakage appeared on the sidewall edge, which showed numerous inflection points with varying degrees of undulation as the irregular profile curve in Fig. 13a, c, e, and g. Correspondingly, when $a_p = 0.04$ mm and $a_p = 0.06$ mm, the edge of the slot sidewall in UVASM is clear and complete, showing a uniform material removal trace and a straight line with better parallelism as regular profile curve in Figs. 12b, d, f, and h and 13b, d, f, and h. When $a_p = 0.08$ mm and $a_p = 0.10$ mm, the edge breakage phenomenon also appears

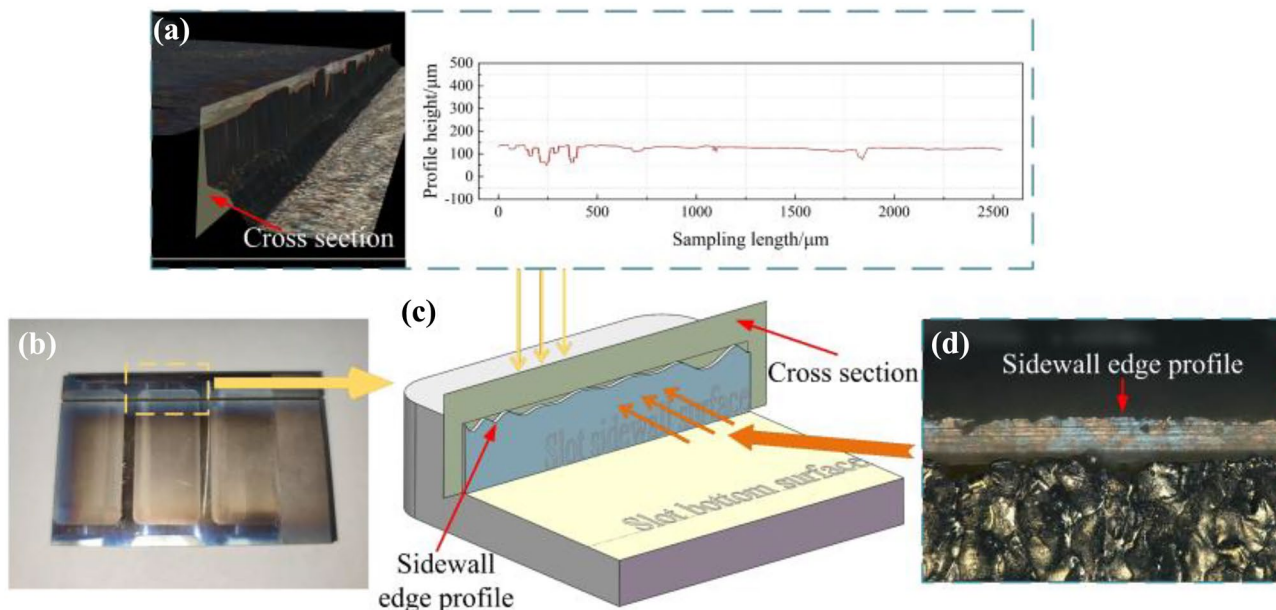


Fig. 10 Schematic diagram of the slot sidewall observation

Fig. 11 Surface texture of slot sidewall under different machining conditions: **a** $v_f=100$ mm/min, CSM, **b** $v_f=100$ mm/min, UVASM, **c** $v_f=400$ mm/min, CSM, and **d** $v_f=400$ mm/min, UVASM (exp. no. 1 and no. 4)

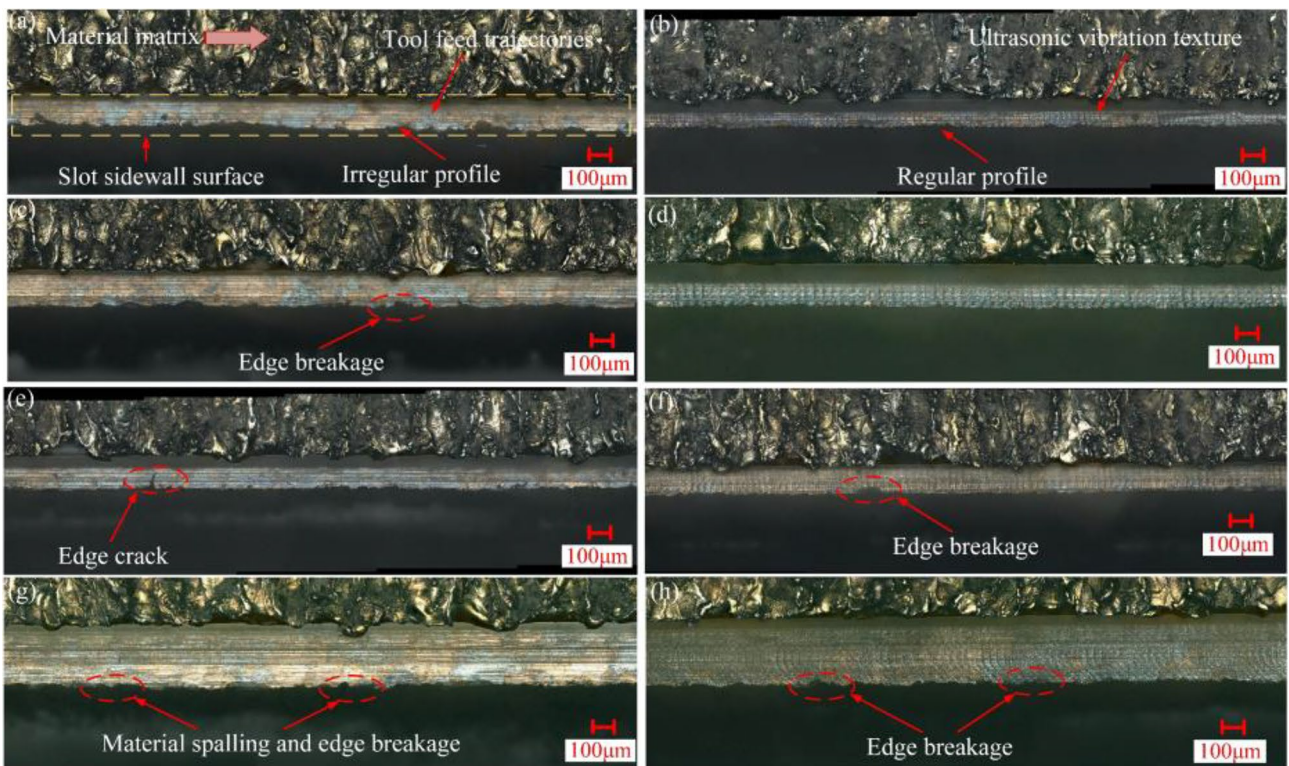
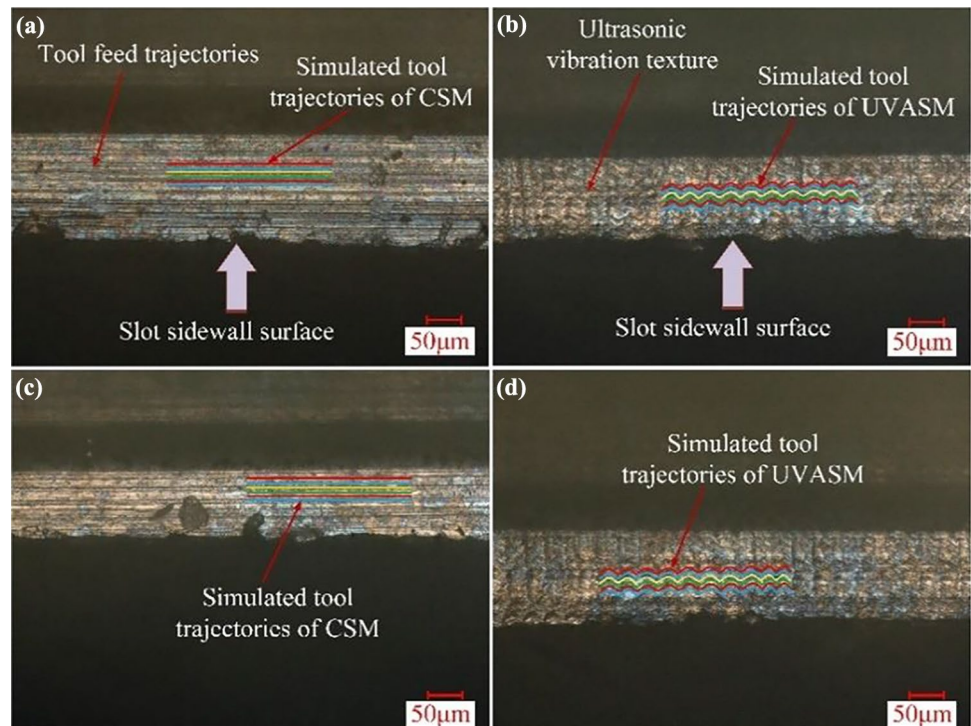


Fig. 12 Topography of slot sidewall edge under different machining conditions: **a** $a_p=0.04$ mm, CSM, **b** $a_p=0.04$ mm, UVASM, **c** $a_p=0.06$ mm, CSM, **d** $a_p=0.06$ mm, UVASM, **e** $a_p=0.08$ mm,

CSM, **f** $a_p=0.08$ mm, UVASM, **g** $a_p=0.10$ mm, CSM, and **h** $a_p=0.10$ mm, UVASM (exp. no. 5, no. 2, no. 6, and no. 7)

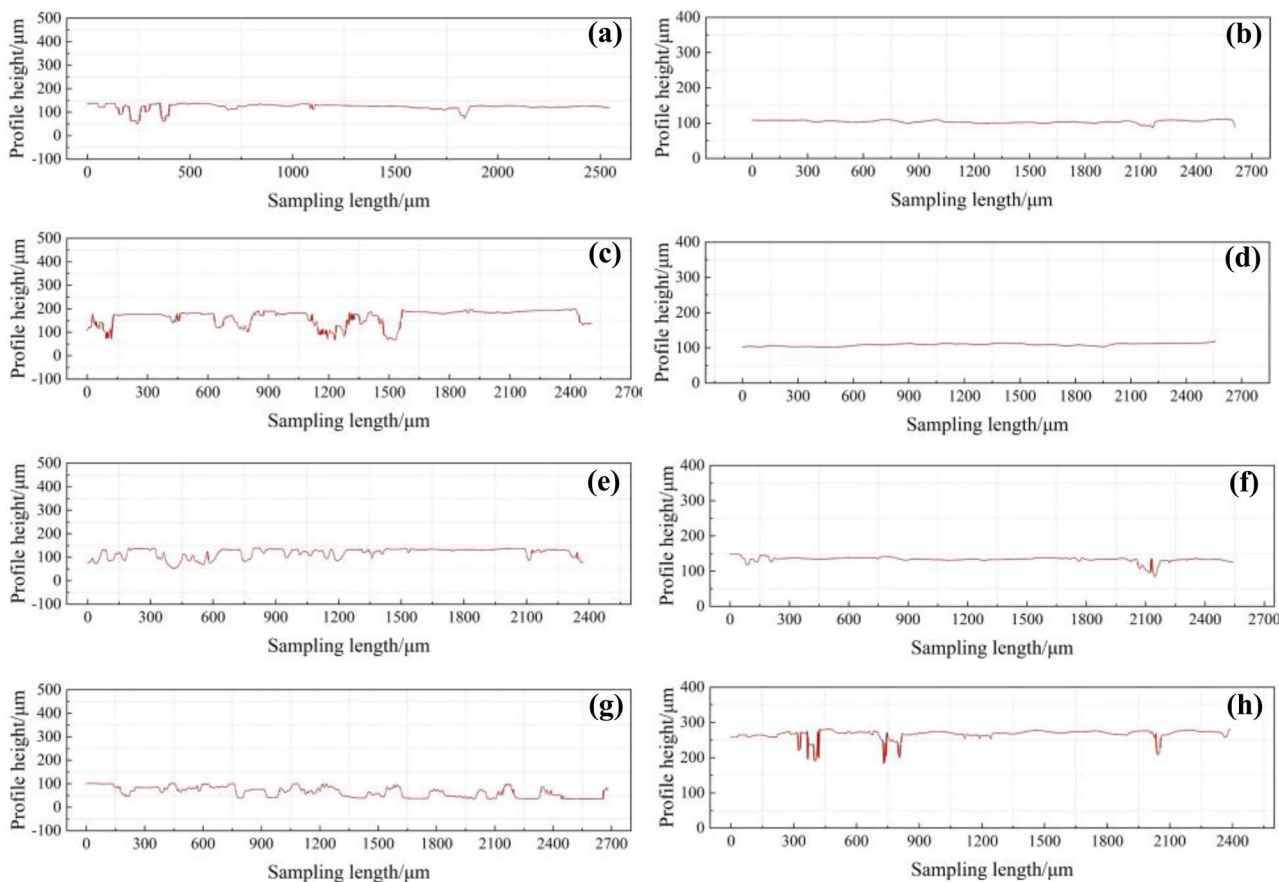


Fig. 13 Profile curve of slot sidewall edge under different machining conditions: **a** $a_p=0.04$ mm, CSM, **b** $a_p=0.04$ mm, UVASM, **c** $a_p=0.06$ mm, CSM, **d** $a_p=0.06$ mm, UVASM, **e** $a_p=0.08$ mm,

CSM, **f** $a_p=0.08$ mm, UVASM, **g** $a_p=0.10$ mm, CSM, and **h** $a_p=0.10$ mm, UVASM (exp. no. 5, no. 2, no. 6, and no. 7)

on the sidewall edge, but its quantity and degree are much smaller than that of CSM under the same parameters.

As mentioned in Sect. 4.2.1, the cutting edge performs high-frequency intermittent milling with a sinusoidal trajectory forming the dynamic cutting thickness and the reduction of cutting force in UVASM. Therefore, the edge material of slot sidewall can be removed uniformly with a smaller amount of removal, which greatly reduces the phenomenon of material spalling and edge breakage. The improvement mechanism can be explained by the combined advantages of dynamic cutting thickness, intermittent machining, and small cutting force in UVASM.

4.3 Morphological characteristics of chips

The collected chips were cleaned with alcohol by the ultrasonic cleaner to remove the cutting fluid attached to the chip’s surface. As shown in Fig. 15, the chips surface in CSM show obvious tool feed trajectories, while that of UVASM shows uniform ultrasonic vibration micro-textures. The surface textures of chips in UVASM and CSM are

highly consistent with that shown in Fig. 11. In addition, it is found that the chip’s edges in UVASM show a uniform jagged profile, and their positions are in good agreement with the ultrasonic vibration textures of the chip’s surface. As shown in Fig. 14, the jagged cutting marks will be left on the chip edges when the cutter tip cuts into the workpiece.

The chip edges show irregular profiles and different material removal phenomena with the increase of cutting depth in CSM. As shown in Fig. 15b-d, when $a_p=0.06$ mm and $a_p=0.08$ mm, the chip edges begin to spall off resulting in the disordered edge profile. When $a_p=0.10$ mm, the chip edges appear material accumulation and tearing phenomena due to irregular material removal. Correspondingly, when $a_p=0.10$ mm, the increase of cutting depth leads to the loss or stacking of sawtooth on the jagged edges of chips in UVASM showing an uneven jagged edge phenomenon.

Comparing the chip morphologies under the two processing methods, it can be found that the length of the chips in UVASM is smaller than that in CSM and the regularity and uniformity of the shape of the chips are higher than that in CSM. The uniformity and shortness of

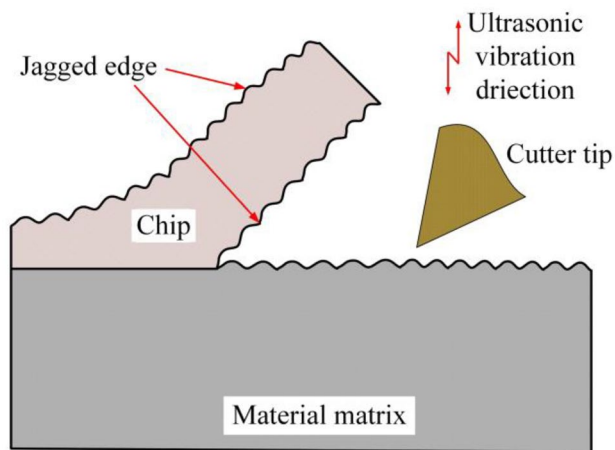


Fig. 14 Schematic diagram of jagged chip formation

the chips also reflect the uniformity and thoroughness of the workpiece material removal process. Short chips are more likely to be taken away by cutting fluid in the milling process, which represents fewer surface scratches. This conclusion is very consistent with Fig. 5. Combined with the description in Sect. 2, the chips in UVASM are also subjected to additional cutting force F_U during the removal process and the cutting thickness is also dynamically changing, so it is easier to obtain shorter chips than that in CSM. In summary, it can be concluded that the unique high-frequency intermittent processing method in UVASM has a better chip breaking effect and surface anti-scratch effect.

4.4 Subsurface microstructure

The specimens are first polished with different grit sandpaper and then etched using an etching solution with a volume ratio of $\text{HF}:\text{HNO}_3:\text{H}_2\text{O} = 1:1:5$ in order to etch out the grain boundaries on the surface of the material for observation. Figure 16 shows the sub-surface microstructure of the specimen cross-section perpendicular to the feed direction as observed by scanning electron microscopy (SEM). The material subsurface can be divided into two zones: the plastic deformation zone and the bulk material zone. The bulk material zone is defined as the material part that was not impacted by the cutting tool with sparse microstructure, while the plastic deformation zone is defined as the material part that was impacted by the cutting tool with tight microstructure. It is observed that the width of the plastic deformation zone in UVASM is larger than that in CSM. The reason is that the workpiece surface is not only extruded by the tool but also hammered by the axial ultrasonic in UVASM, while the workpiece surface is only extruded by the tool in CSM. Therefore, under the dual action, the subsurface microstructure is tighter and wider in UVASM than that of CSM.

It is generally accepted that the hardened surface is the result of work hardening caused by plastic deformation during the cutting process [39, 40]. The thickness of the plastic deformation layer represents the degree of work hardening. The results show that the UVASM can obtain a deeper plastic deformation layer, which indicates that it can have higher work hardening and surface micro-hardness.

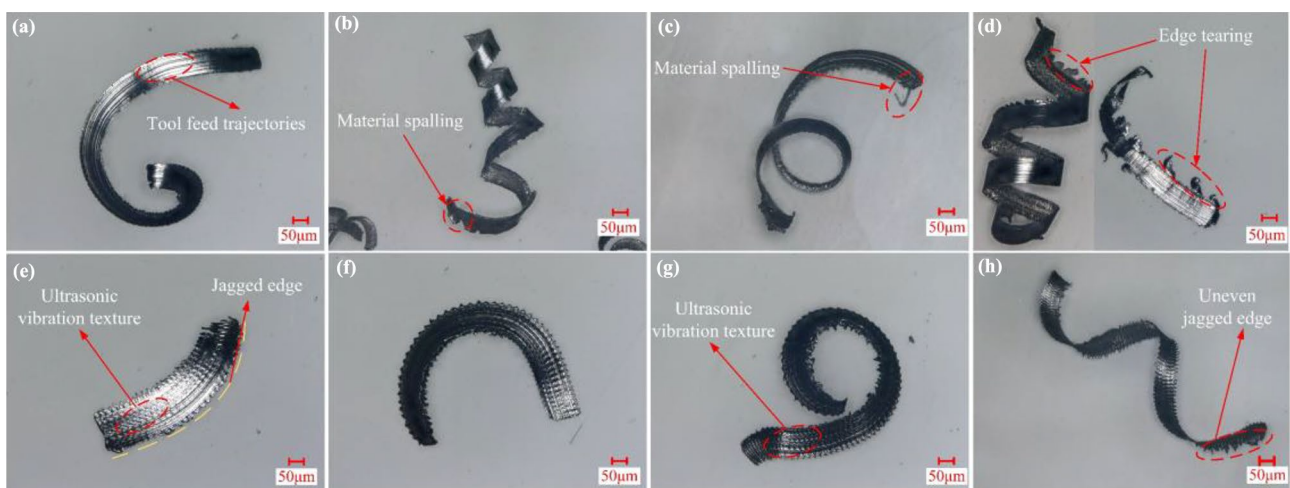
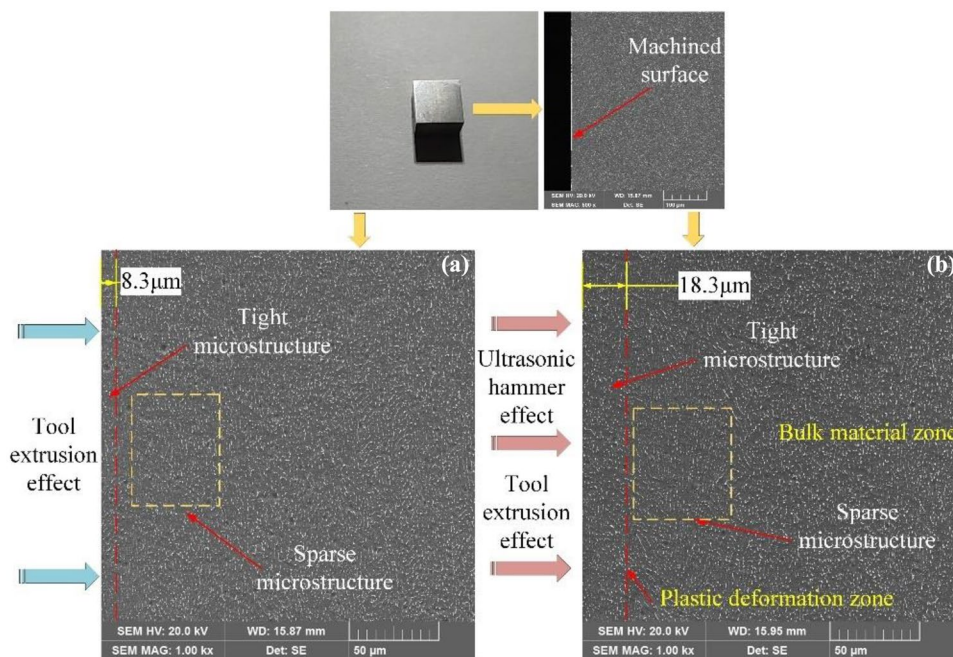


Fig. 15 Comparison of chip morphology under different machining conditions: **a** $a_p=0.04$ mm, CSM, **b** $a_p=0.06$ mm, CSM, **c** $a_p=0.08$ mm, CSM, **d** $a_p=0.10$ mm, CSM, **e** $a_p=0.04$ mm,

UVASM, **f** $a_p=0.06$ mm, UVASM, **g** $a_p=0.08$ mm, UVASM, and **h** $a_p=0.10$ mm, UVASM (exp. no. 5, no. 2, no. 6, and no. 7)

Fig. 16 Microstructure of the subsurface layer: **a** CSM and **b** UVASM (exp. no. 2)



4.5 Micro-hardness

Micro-hardness is usually determined by the coupling effect of mechanical and thermal loads. High micro-hardness represents the ability of a material to resist residual deformation and damage. The micro-hardness of the surface and subsurface was tested, as shown in Figs. 17 and 19, in order to investigate the mechanical characteristics of the machined surface. The micro-hardness of each parameter was measured three times, and the average value was taken as the hardness for the different machined surfaces. The bulk material micro-hardness value is approximately 366 HV.

Figure 17 shows the corresponding relationship between the surface micro-hardness and the cutting width, cutting depth, feed speed, and ultrasonic power factor in UVASM and CSM. As shown in Fig. 17a-c, the surface micro-hardness in UVASM and CSM are both higher than the hardness of the bulk material, and the surface micro-hardness of UVASM is higher than that of CSM. In Fig. 17a, the surface micro-hardness of CSM continuously decreases with the increase of the cutting width, while the surface micro-hardness in UVASM shows an overall upward trend. In Fig. 17b, c, there is no specific change trend of surface micro-hardness in the two processing methods. In Fig. 17d, the surface micro-hardness first increases and then decreases as the power factor increases. And when the power factor is 60 and 90%, its micro-hardness is less than that of CSM. The results show that the relatively high micro-hardness can be obtained when the power factor is 80%.

According to the above analysis, it can be concluded that work hardening exists in both processing methods. This is because of the extrusion and friction of the cutting edge on the

material during the milling process, which causes the plastic deformation and hardening of the machined surface. The tool attached with axial ultrasonic vibration in UVASM continuously hammers the workpiece surface, resulting in an increase in the micro-hardness value. In addition, the high-frequency intermittent cutting mode in UVASM brings additional rubbing, burnishing, and the cutting-extrusion effects, which increases the surface micro-hardness.

The measurement area in the specimen and micro-indentation array in the subsurface is illustrated in Fig. 18. The first micro-hardness measurement of the subsurface was taken at the depth of 50 μm beneath the machined surface. Afterward, each row was offset 80 μm in the depth direction until 615 μm beneath the machined surface, and the distance between each column was 100 μm. As illustrated in Fig. 19, the micro-hardness of the subsurface in both processing methods generally decreases with the increase of depth. Moreover, the micro-hardness of the subsurface in UVASM is significantly higher than that in CSM at different depths except that the depth is equal to 455 μm, which can be attributed to the enhanced work hardening caused by the application of ultrasonic vibration.

In addition, it is found that the subsurface micro-hardness at 375 μm below the machined surface in UVASM is less than the hardness of the bulk material, while that of CSM is at 295 μm. This shows that the UVASM can obtain a thicker plastic deformation layer, which is the same as the conclusion obtained in Sect. 4.4. It can also be observed that the micro-hardness values drop to micro-hardness values (366 HV) of bulk material beyond the depth of about 295 and 375 μm in CSM and UVASM, respectively, which indicates that no significant work hardening effect beyond this depth.

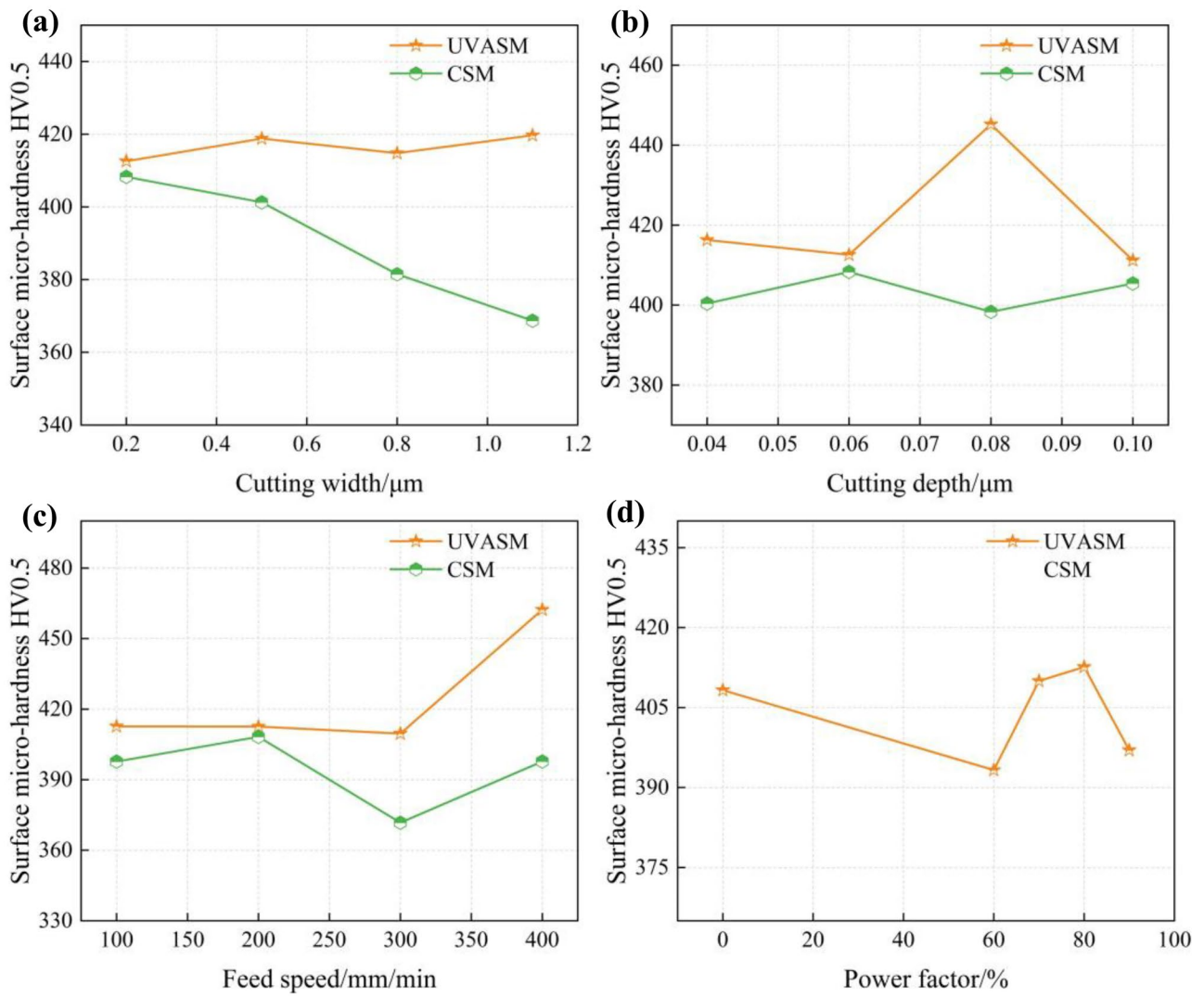


Fig. 17 Surface micro-hardness under different machining methods and parameters

Fig. 18 Micro-indentation array in the subsurface (exp. no. 2)

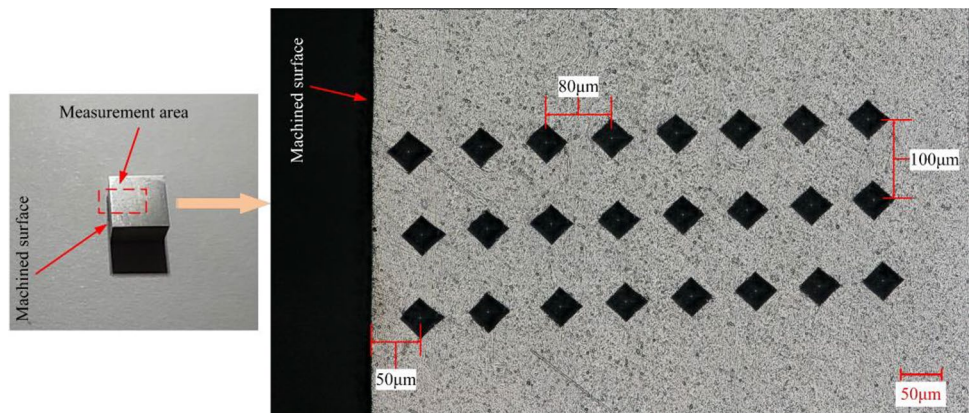
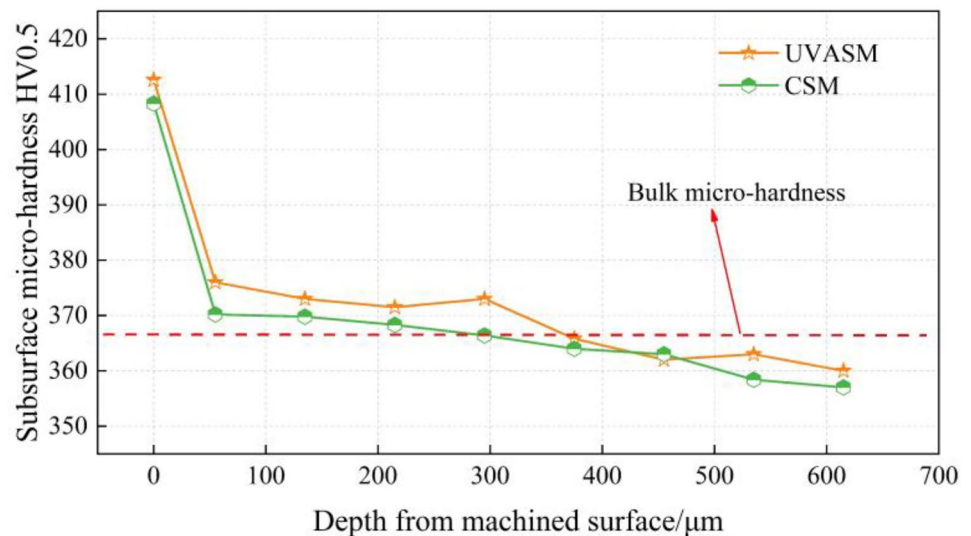


Fig. 19 Variation of the micro-hardness beneath the machined surface (exp. no. 2)



5 Conclusions

Through theoretical analysis and experimental research, the processing mechanism and processing effect of UVASM and CSM of titanium alloys were investigated comparatively and the surface feature and material removal characteristics were analyzed from different aspects. The following conclusions can be drawn:

1. The tool-workpiece experience different contact states within a vibration cycle, resulting in a high-frequency intermittent contact mode during the UVASM process. The additional cutting force F_U caused by the axial ultrasonic vibration will easily generate short chips due to the chip breaking effect.
2. The material can be removed evenly and completely with the motion trajectory of the cutting edge and the ultrasonic vibration trajectory in the slot bottom of UVASM. The uniform micro-textures in UVASM can significantly improve the surface topography, while numerous disordered tool trajectories, scratches, and machining defects detract from the surface quality in CSM.
3. The tool tip trajectories of the two machining methods highly correspond to the machining textures of slot sidewall surfaces, respectively. The UVASM method can greatly reduce the phenomenon of material spalling and edge breakage to form a regular and complete edge profile of slot sidewall.
4. The milling force waveform in UVASM has a high-frequency and small-amplitude force fluctuation signal on the original periodic vibration waveform. The instantaneous maximum milling force, duration of the initial cutting stage, and milling force in a stable stage in UVASM are reduced by 8.7%, 42.9%, and 12.2% compared with those of CSM, respectively.
5. The chip morphologies of UVASM are distributed with uniform vibration micro-textures and jagged profiles, while those of CSM are distributed with tool feed trajectories and irregular profiles. The chip size of UVASM is much smaller than that of CSM, and the regularity and uniformity of the shape of the chips are higher than that in CSM due to the chip breaking effect. The additional rubbing, burnishing, and cutting-extrusion effects generate higher micro-hardness and deeper plastic deformation layer in UVASM. In summary, the multi-dimensional evaluation of slot processing status has been completed, and the processing quality of the slot has been improved with optimized cutting parameters ($v_f=400$ mm/min, $a_p=0.06$ mm, $a_e=1.1$ mm, and $p=80\%$).

Author contribution All authors contributed to the study's conception and design. Material preparation and data collection were performed by Baoqi Chang and Zhaoxi Yi. Ji-an Duan and Xiaobing Cao participated in the data analysis and logical analysis of the article. The first draft of the manuscript was written by Baoqi Chang, and all authors commented on previous versions of the manuscript. All authors read and approved the final manuscript.

Funding This study was supported by the Fundamental Research Funds for the Central Universities of Central South University (no. 2021zzts0130).

Data availability The datasets used or analyzed during the current study are available from the corresponding author on reasonable request.

Code availability Not applicable.

Declarations

Ethics approval The content studied in this article belongs to the field of ultrasonic processing and does not involve humans and animals. This article strictly follows the accepted principles of ethical and professional conduct.

Consent to participate My co-authors and I would like to opt into In Review.

Consent for publication I agree with the copyright transfer statement.

Competing interests The authors declare no competing interests.

References

- Khalil AK, Yip WS, To S (2022) Theoretical and experimental investigations of magnetic field assisted ultra-precision machining of titanium alloys. *J Mater Process Technol* 300. <https://doi.org/10.1016/j.jmatprotec.2021.117429>
- Aslantas K, Ülker Ş, Şahan Ö, Pimenov DY, Giasin K (2021) Mechanistic modeling of cutting forces in high-speed microturning of titanium alloy with consideration of nose radius. *Int J Adv Manuf Tech*. <https://doi.org/10.1007/s00170-021-08437-w>
- Niu Y, Jiao F, Zhao B, Gao G (2019) Investigation of cutting force in longitudinal-torsional ultrasonic-assisted milling of Ti-6Al-4V. *Materials* 12(12). <https://doi.org/10.3390/ma12121955>
- Yip WS, To S, Sun Z (2021) Hybrid ultrasonic vibration and magnetic field assisted diamond cutting of titanium alloys. *J Manuf Processes* 62:743–752. <https://doi.org/10.1016/j.jmapro.2020.12.037>
- Gao G, Xia Z, Yuan Z, Xiang D, Zhao B (2021) Influence of longitudinal-torsional ultrasonic-assisted vibration on micro-hole drilling Ti-6Al-4V. *Chin J Aeronaut* 34(9):247–260. <https://doi.org/10.1016/j.cja.2020.06.012>
- Thepsonthi T, Özel T (2012) Multi-objective process optimization for micro-end milling of Ti-6Al-4V titanium alloy. *Int J Adv Manuf Tech* 63(9–12):903–914. <https://doi.org/10.1007/s00170-012-3980-z>
- Rinck PM, Gueray A, Kleinwort R, Zaeh MF (2020) Experimental investigations on longitudinal-torsional vibration-assisted milling of Ti-6Al-4V. *Int J Adv Manuf Tech* 108(11–12):3607–3618. <https://doi.org/10.1007/s00170-020-05392-w>
- Du Y, Yue C, Li X, Liu X, Liang SY (2021) Research on breakage characteristics in side milling of titanium alloy with cemented carbide end mill. *Int J Adv Manuf Tech* 117(11–12):3661–3679. <https://doi.org/10.1007/s00170-021-07938-y>
- Abdo BMA, Anwar S, El-Tamimi A (2019) Machinability study of biolox forte ceramic by milling microchannels using rotary ultrasonic machining. *J Manuf Processes* 43:175–191. <https://doi.org/10.1016/j.jmapro.2019.05.031>
- Kumar J (2014) Investigations into the surface quality and micro-hardness in the ultrasonic machining of titanium (ASTM GRADE-1). *J Braz Soc Mech Sci Eng* 36(4):807–823. <https://doi.org/10.1007/s40430-014-0130-6>
- Zhao B, Chang BQ, Yuan LS, Li PT (2019) Influence of force load on the stability of ultrasonic longitudinal-torsional composite drilling system. *Int J Adv Manuf Tech* 106(3–4):891–905. <https://doi.org/10.1007/s00170-019-04654-6>
- Fang B, Yuan Z, Li D, Gao L (2021) Effect of ultrasonic vibration on finished quality in ultrasonic vibration assisted micromilling of Inconel718. *Chin J Aeronaut* 34(6):209–219. <https://doi.org/10.1016/j.cja.2020.09.021>
- Zhu LD, Ni CB, Yang ZC, Liu CF (2019) Investigations of micro-textured surface generation mechanism and tribological properties in ultrasonic vibration-assisted milling of Ti-6Al-4V. *Precis Eng* 57:229–243. <https://doi.org/10.1016/j.precisioneng.2019.04.010>
- Ni CB, Zhu LD, Yang ZC (2019) Comparative investigation of tool wear mechanism and corresponding machined surface characterization in feed-direction ultrasonic vibration assisted milling of Ti-6Al-4V from dynamic view. *Wear* 436–437. <https://doi.org/10.1016/j.wear.2019.203006>
- Jain A, Singh G, Jain V, Gupta D (2020) Feasibility analysis for machining serpentine microchannels on glass using rotary ultrasonic milling. *Meas* 160. <https://doi.org/10.1016/j.measurement.2020.107844>
- Ahmed F, Ko TJ, Kurniawan R, Kwack Y (2021) Machinability analysis of difficult-to-cut material during ultrasonic vibration-assisted ball end milling. *Mater Manuf Processes* 36(15):1734–1745. <https://doi.org/10.1080/10426914.2021.1944194>
- Baraheni M, Amini S (2019) Investigation on rotary ultrasonic assisted end grinding of silicon nitride ceramics. *SN Appl Sci* 1(12). <https://doi.org/10.1007/s42452-019-1594-x>
- Sajjady SA, Abadi HNH, Amini S, Nosouhi R (2016) Analytical and experimental study of topography of surface texture in ultrasonic vibration assisted turning. *Mater Des* 93:311–323. <https://doi.org/10.1016/j.matdes.2015.12.119>
- Ding H, Ibrahim R, Kai C, Chen SJ (2010) Experimental study on machinability improvement of hardened tool steel using two dimensional vibration-assisted micro-end-milling. *Int J Mach Tools Manuf* 50(12):1115–1118
- Lu H, Zhu LD, Yang ZC, Lu H, Yan BL, Hao YP, Qin SQ (2021) Research on the generation mechanism and interference of surface texture in ultrasonic vibration assisted milling. *Int J Mech Sci* 208. <https://doi.org/10.1016/j.ijmecsci.2021.106681>
- Ni CB, Zhu LD (2020) Investigation on machining characteristics of TC4 alloy by simultaneous application of ultrasonic vibration assisted milling (UVAM) and economical-environmental MQL technology. *J Mater Process Technol* 278. <https://doi.org/10.1016/j.jmatprotec.2019.116518>
- Chen WQ, Zheng L, Xie WK, Yang K, Huo DH (2019) Modelling and experimental investigation on textured surface generation in vibration-assisted micro-milling. *J Mater Process Technol* 266:339–350. <https://doi.org/10.1016/j.jmatprotec.2018.11.011>
- Liu JJ, Jiang XG, Han X, Gao Z, Zhang DY (2018) Effects of rotary ultrasonic elliptical machining for side milling on the surface integrity of Ti-6Al-4V. *Int J Adv Manuf Tech* 101(5–8):1451–1465. <https://doi.org/10.1007/s00170-018-2847-3>
- Chen G, Ren CZ, Zou YH, Qin XD, Lu LP, Li SP (2019) Mechanism for material removal in ultrasonic vibration helical milling of Ti 6Al 4V alloy. *Int J Mach Tools Manuf* 138:1–13. <https://doi.org/10.1016/j.ijmachtools.2018.11.001>
- Barry J, Byre J, Lennon D (2001) Observations on chip formation and acoustic emission in machining Ti-6Al-4V alloy. *Int J Mach Tools Manuf* 41:1055–1070
- Sun S, Brandt M, Dargusch MS (2009) Characteristics of cutting forces and chip formation in machining of titanium alloys. *Int J Mach Tools Manuf* 49(7–8):561–568. <https://doi.org/10.1016/j.ijmachtools.2009.02.008>
- Moghaddas A (2021) Characterization of thrust force, temperature, chip morphology and power in ultrasonic-assisted drilling of aluminium 6061. *Int J Adv Manuf Tech*. <https://doi.org/10.1007/s00170-021-07742-8>
- Jung HJ, Hayasaka T, Shamoto E, Xu LJ (2020) Suppression of forced vibration due to chip segmentation in ultrasonic elliptical vibration cutting of titanium alloy Ti-6Al-4V. *Precis Eng* 64:98–107. <https://doi.org/10.1016/j.precisioneng.2020.03.017>
- Ren WF, Xu JK, Lin JQ, Yu ZJ, Yu P (2019) Research on homogenization and surface morphology of Ti-6Al-4V alloy by longitudinal-torsional coupled ultrasonic vibration ball-end milling. *Int J Adv Manuf Tech* 104:301–313. <https://doi.org/10.1007/s00170-019-03668-4>
- Yang D, Liu Z (2017) Surface integrity generated with peripheral milling and the effect on low-cycle fatigue performance of aeronautical titanium alloy Ti-6Al-4V. *The Aeronautical Journal* 122(1248):316–332. <https://doi.org/10.1017/aer.2017.136>
- Abbasi SA, Feng P, Ma Y, Zhang J, Yu D, Wu Z (2016) Influence of microstructure and hardness on machinability of heat-treated

- titanium alloy Ti-6Al-4V in end milling with polycrystalline diamond tools. *Int J Adv Manuf Tech* 86(5–8):1393–1405. <https://doi.org/10.1007/s00170-015-8245-1>
32. Chen G, Zou YH, Qin XD, Liu J, Feng Q, Ren CZ (2020) Geometrical texture and surface integrity in helical milling and ultrasonic vibration helical milling of Ti-6Al-4V alloy. *J Mater Process Technol*. <https://doi.org/10.1016/j.jmatprotec.2019.116494>
33. Niu Y, Jiao F, Zhao B, Wang D (2017) Multiobjective optimization of processing parameters in longitudinal-torsion ultrasonic assisted milling of Ti-6Al-4V. *Int J Adv Manuf Tech* 93(9–12):4345–4356. <https://doi.org/10.1007/s00170-017-0871-3>
34. Lesyk DA, Martinez S, Mordyuk BN, Dzhemelinskyi VV, Lamikiz A, Prokopenko GI (2019) Effects of laser heat treatment combined with ultrasonic impact treatment on the surface topography and hardness of carbon steel AISI 1045. *Opt Laser Technol* 111:424–438. <https://doi.org/10.1016/j.optlastec.2018.09.030>
35. Ying N, Feng J, Bo Z, Guofu G, Jing-jing N (2020) Theoretical investigation of machining-induced residual stresses in longitudinal torsional ultrasonic-assisted milling. *Int J Adv Manuf Tech* 108(11–12):3689–3705. <https://doi.org/10.1007/s00170-020-05495-4>
36. Li H, He GY, Qin XD, Wang GF, Lu C, Gui LJ (2014) Tool wear and hole quality investigation in dry helical milling of Ti-6Al-4V alloy. *Int J Adv Manuf Tech* 71(5–8):1511–1523. <https://doi.org/10.1007/s00170-013-5570-0>
37. Zou YH, Chen G, Lu LP, Qin XD, Ren CZ (2019) Kinematic view of cutting mechanism in hole-making process of longitudetorsional ultrasonic assisted helical milling. *Int J Adv Manuf Tech* 103(1–4):267–280. <https://doi.org/10.1007/s00170-019-03483-x>
38. Nath C, Rahman M (2008) Effect of machining parameters in ultrasonic vibration cutting. *Int J Mach Tools Manuf* 48(9):965–974. <https://doi.org/10.1016/j.ijmactools.2008.01.013>
39. Li X, Zhao P, Niu Y, Guan C (2016) Influence of finish milling parameters on machined surface integrity and fatigue behavior of Ti1023 workpiece. *Int J Adv Manuf Tech* 91(1–4):1297–1307. <https://doi.org/10.1007/s00170-016-9818-3>
40. Teimouri R, Liu Z (2020) An analytical prediction model for residual stress distribution and plastic deformation depth in ultrasonic-assisted single ball burnishing process. *Int J Adv Manuf Tech* 111(1–2):127–147. <https://doi.org/10.1007/s00170-020-06068-1>

Publisher's Note Springer Nature remains neutral with regard to jurisdictional claims in published maps and institutional affiliations.

Springer Nature or its licensor holds exclusive rights to this article under a publishing agreement with the author(s) or other rightsholder(s); author self-archiving of the accepted manuscript version of this article is solely governed by the terms of such publishing agreement and applicable law.